

Testing stellar evolution with asteroseismic inversions of a main sequence star harboring a small convective core

EARL P. BELLINGER,<sup>1,\*</sup> SARBANI BASU,<sup>2</sup> SASKIA HEKKER,<sup>3,1</sup> AND JØRGEN CHRISTENSEN-DALSGAARD<sup>1</sup>

<sup>1</sup>*Stellar Astrophysics Centre, Department of Physics and Astronomy, Aarhus University, Denmark*

<sup>2</sup>*Department of Astronomy, Yale University, New Haven, CT, USA*

<sup>3</sup>*Max Planck Institute for Solar System Research, Göttingen, Germany*

(Received December 5, 2021; Revised December 5, 2021; Accepted December 5, 2021)

Submitted to ApJ

## ABSTRACT

The goal of stellar evolution theory is to predict the structure of stars throughout their lifetimes. Usually, these predictions can be assessed only indirectly, for example by comparing predicted and observed effective temperatures and luminosities. Thanks now to asteroseismology, which can reveal the internal structure of stars, it becomes possible to compare the predictions from stellar evolution theory to actual stellar structures. In this work, we present an inverse analysis of the oscillation data from the solar-type star KIC 6225718, which was observed by the *Kepler* space observatory during its nominal mission. As its mass is about 20% greater than solar, this star is predicted to transport energy by convection in its nuclear-burning core. We find significant differences between the predicted and actual structure of the star in the radiative interior near to the convective core. In particular, the predicted sound speed is higher than observed in the deep interior of the star, and too low at a fractional radius of 0.25 and beyond. The cause of these discrepancies is unknown, and is not remedied by known physics in the form of convective overshooting or elemental diffusion.

*Keywords:* asteroseismology — stars: evolution, interiors, solar-type, individual (KIC 6225718)

## 1. INTRODUCTION

Asteroseismology provides the unique opportunity to learn about the internal properties of stars through their global modes of oscillation. This is often achieved by fitting theoretical stellar models to observations of a star, and then assuming the best model to be a proxy for the star (for an introduction to stellar modeling with asteroseismology, see Basu & Chaplin 2017). However, even the best theoretical models currently fail to match all of the asteroseismic signals that are observed in stars exhibiting solar-like oscillations, even after applying corrections for near-surface effects (e.g., Ball & Gizon 2014, and references therein). This implies that the internal structure of models of solar-like stars are not exactly right, and motivates the need for another approach.

The oscillations that are observed in low-mass main sequence stars like the Sun travel as sound waves through the stellar interior (for an overview of asteroseismology, see Aerts et al. 2010). As such, at each point in the interior these waves propagate at the local speed of sound, the square of which is proportional to the ratio of the pressure to density at that location in the stellar interior. When enough modes are observed, it becomes possible to map out the speed of sound at various points in the stellar interior, and thus infer the structure of the star. This analysis is referred to as a *structure inversion*, as it is inverse to the forward problem of calculating the oscillation frequencies of a known stellar structure.

Structure inversions are typically carried out by inferring the differences in internal structure between the star and a given model, called the reference model, through an inspection of the differences in their oscillation frequencies. This can be achieved by linearizing the perturbed stellar oscillation equations around the reference model (Gough 1985; Gough & Thompson 1991). When the reference model is the best-fitting stellar evolution

Corresponding author: Earl P. Bellinger  
bellinger@phys.au.dk

\* SAC Postdoctoral Fellow



model, a structure inversion leads directly to an evaluation of whether stellar evolution theory produces the correct stellar structure within the uncertainty of the inversion result.

In the case of the Sun, for which there is rich helioseismic data, structure inversions have provided numerous constraints on the physics of the solar interior (see Basu 2016 for a review). For example, Christensen-Dalsgaard et al. (1993) compared the actual solar structure as inferred by seismic inversion to standard solar models which were calculated both with and without considering the effects of element diffusion. They found that the inclusion of diffusion deepened the convective envelope, which ultimately resulted in a reduction of the discrepancy between theory and observation in the internal adiabatic sound speed profile by a factor of three, from a maximum difference of about 0.6% down to about 0.2%. Similarly, Basu & Christensen-Dalsgaard (1997) compared solar models that were constructed using different equations of state, and from this investigation they were able to rule out the Eggleton, Faulkner & Flannery (EFF, 1973) EOS for solar matter. Although even today there remain highly significant discrepancies between the structure of solar models and the actual structure of the Sun, these analyses confirmed that solar models are nevertheless extremely accurate in an absolute sense.

Thanks to the high-quality asteroseismic data collected by the NASA *Kepler* space observatory (Borucki et al. 2010), we have the first opportunity to perform similar tests of internal physics on other stars. There are however important differences between helioseismic and asteroseismic data, at least at the present time. Because the solar disk can be resolved, thousands of modes of high spherical degree ( $\ell \lesssim 250$ ) can be observed in the Sun. In stars, on the other hand, geometrical cancellation restricts observations to, at most, dozens of global modes ( $\ell \leq 3$ ). Fortunately, nearly all of these modes traverse nearly all of the stellar interior, thereby providing constraints on the nature of the stellar core. The structure of stellar envelopes, on the other hand, are insensitive to asteroseismic characterization, at least at the present time. Another important difference is that we have accurate and precise independent knowledge of the fundamental solar parameters (age, mass, radius). For other stars, these must be estimated—usually also from the asteroseismic data—leading to large uncertainty in the results.

Recently, Bellinger et al. (2017) introduced a technique to overcome these challenges by inverting an array of reference models spanning the uncertainties in the stellar mass and radius. Using this technique it was

**Table 1.** Observed Parameters of KIC 6225718

Parameter	Value	Unit
$T_{\text{eff}}$	$6313 \pm 77$	K
[Fe/H]	$-0.07 \pm 0.10$	
$\nu_{\text{max}}$	$2369 \pm 24$	$\mu\text{Hz}$
$\Delta\nu$	$105.754 \pm 0.096$	$\mu\text{Hz}$

*Notes.* Rows contain the effective temperature, metallicity, frequency at maximum oscillation power, and large frequency separation. Values adopted from Lund et al. (2017).

possible to resolve the radial structure of the cores in the two solar-like stars belonging to the 16 Cygni system. The uncertainties in the inversion result were large, however, making it difficult to assess whether there were important differences between the structure of the stars and the predictions of stellar evolution theory.

In this paper, we take another approach, which was outlined in anticipation of first asteroseismic data by Basu (2003). Instead of determining the dimensional structure of a star, the precision of which is highly impacted by the uncertainties in the stellar mass and radius, we rather seek its dimensionless structure. The star we have selected for this analysis is KIC 6225718, also known in the literature as Saxo2, which is one of the best solar-type stars observed by *Kepler* (Lund et al. 2017). Like the Sun and 16 Cyg A and B, it is a slow rotator, with a projected rotational velocity of  $2.4 \pm 0.5$  km/s (Molenda-Żakowicz et al. 2013). Other observational constraints for this star are listed in Table 1. Unlike the Sun and 16 Cyg A and B, this star is just massive enough for stellar evolution theory to predict it to harbor a small convective core on the main sequence (Bellinger et al. 2019; Bellinger 2019). Thus it constitutes an interesting testbed for furthering our understanding of stellar physics.

## 2. EVOLUTIONARY MODELLING

The first step of the analysis is to obtain a suitable reference model for KIC 6225718. We used the *Stellar Parameters in an Instant* (SPI, Bellinger et al. 2016; Angelou et al. 2017) method to estimate the fundamental parameters of KIC 6225718 and subsequently obtained a model according to those parameters. Briefly, this method uses machine learning with theoretical stellar models to determine which parameters (mass, age, initial chemical composition, mixing length parameter, etc.) are most consistent with the observations of a given star. As this method requires a grid of models, we used *Modules for Experiments in Stellar Astrophysics* (MESA r10108, Paxton et al. 2011, 2013, 2015, 2018, 2019) for the evolution calculations. We calculated 1024 tracks with initial condi-



**Table 2.** Estimated Parameters of KIC 6225718

Parameter	Estimate	Ref. Mod.	Solar	Unit
Age	$3.09 \pm 0.63$	2.803	4.572	Gyr
Mass	$1.189 \pm 0.053$	1.20	1	$M_{\odot}$
Radius	$1.25 \pm 0.024$	1.24	1	$R_{\odot}$
$X_c$	$0.287 \pm 0.053$	0.30	0.34	—
$X_0$	$0.7080 \pm 0.0059$	0.71	0.70	—
$Z_0$	$0.0202 \pm 0.0031$	0.021	0.019	—
$\alpha_{MLT}$	$2.04 \pm 0.14$	2.05	1.84	—

*Notes.* The quantity  $X_c$  refers to the fractional hydrogen abundance in the core of the model, which is a proxy for its main-sequence age. The quantities  $X_0$  and  $Z_0$  refer to the initial hydrogen abundance and initial metallicity, respectively. The quantity  $\alpha_{MLT}$  refers to the mixing length parameter. The values of the reference model as well as those for a solar-calibrated model are provided.

tions varied quasi-randomly using a Sobol generation scheme (see Appendix B of Bellinger et al. 2016). The tracks were varied in mass ( $0.7 \leq M/M_{\odot} \leq 3$ ), initial helium abundance ( $0.22 \leq Y_0 \leq 0.34$ ), initial metallicity ( $0.0001 \leq Z_0 \leq 0.04$  on a uniform logarithmic grid), and mixing length parameter ( $1 \leq \alpha_{MLT} \leq 3$ ). Diffusion and overshoot are not considered at this stage of the analysis, but will be considered later. The remaining aspects of the models are the same as described by Bellinger et al. (2019). We used the mean-shift algorithm (Fukunaga & Hostetler 1975) to find the mode of the joint posterior distribution of the estimated parameters (age, mass, chemical composition, and mixing length parameter, tabulated in Table 2), and used those parameters to compute the reference model.

Figure 1 shows the structure of the reference model. In particular, it shows the internal profile of the isothermal speed of sound  $\sqrt{u}$ , defined as  $u = P/\rho$ , with  $P$  being pressure and  $\rho$  being density. Figure 2 shows an asteroseismic comparison of this model to the observations of KIC 6225718. Two ways of dealing with the surface term are shown: one by applying the Ball & Gizon (2014) two-term correction, and another by inspecting the asteroseismic frequency ratios  $r_{02}$ ,  $r_{13}$ , and  $r_{10}$  (for definitions, see, e.g., Roxburgh & Vorontsov 2003, 2013; Roxburgh 2005, 2018). Significant differences are apparent in 17 of the modes, with the differences in some modes exceeding  $8\sigma$ . In both cases it is clear that the stellar evolution model does not pulsate the same way as does the star. Furthermore, these differences are caused by differences in the internal structure of the star, and not by surface effects. The task is then to find where the internal structure differs.

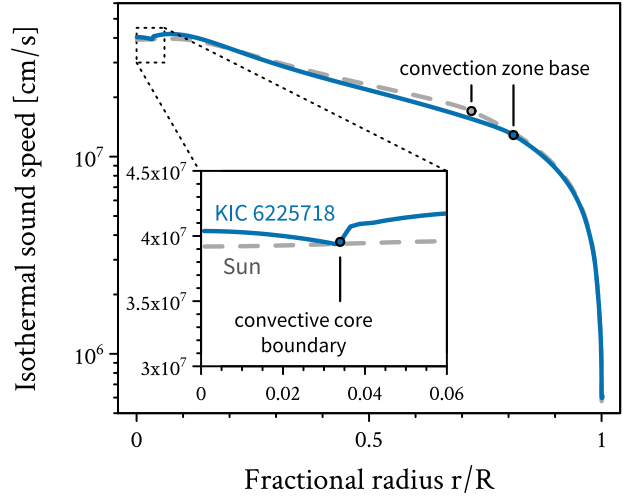


**Figure 1.** The acoustic structure  $\sqrt{u}$  of the best-fitting model for KIC 6225718 as a function of the fractional radius  $r/R$ , where  $r$  is the distance from the stellar center and  $R$  is the total stellar radius. A solar model is shown for reference. The inset diagram shows a zoom-in on the deep stellar interior, where the signature of a convective core is apparent. Convective boundaries are indicated.

### 3. ASTEROSEISMIC INVERSION

We now seek to obtain asteroseismic measurements of the internal sound speed profile so that we may compare the structure of the star with the structure that is predicted from stellar evolution theory. In order to achieve this, we perturb the equations of stellar oscillation and linearize them around the reference model in order to determine how changes to the stellar structure result in changes to the mode frequencies (e.g., Basu & Chaplin 2017). For each mode of oscillation we obtain an equation which relates the difference in the frequency of the mode between the star and the reference model to the differences in their internal structure:

$$\frac{\delta\nu}{\nu} = \int K(u', Y) \frac{\delta u'}{u'} dx + \int K(Y, u') \delta Y dx. \quad (1)$$

Here  $\nu$  is the frequency of the mode,  $\delta\nu$  is the difference in  $\nu$  between the model and the star,  $\delta Y$  is the difference in the fractional abundance of helium, and  $\delta u'$  is the difference in the dimensionless squared isothermal sound speed  $u' = uR/M$ , with  $M$  being the total stellar mass (Basu 2003). The kernels, denoted  $K$ , are computed numerically based on the structure of the reference model (e.g., Gough & Thompson 1991; Kosovichev 1999). These functions quantify how a perturbation to  $u'$  or  $Y$  at any point in the stellar interior will result in a perturbation to  $\nu$ . Examples of these kernels for vari-



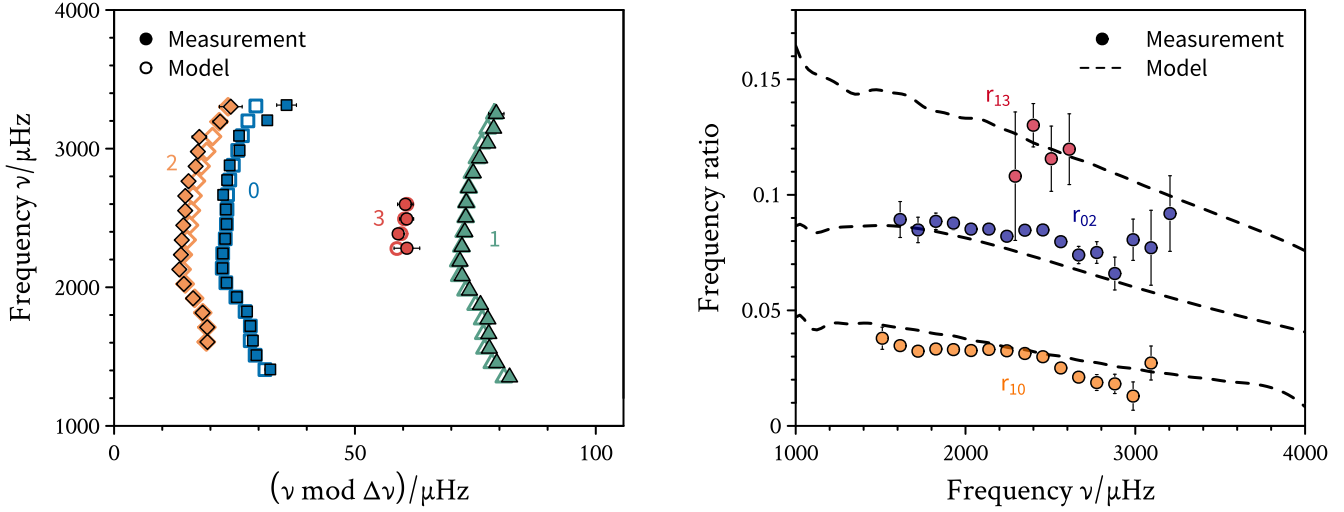


**Figure 2.** Comparisons of predicted and measured seismic properties. **LEFT PANEL.** Échelle diagram comparing the observed frequencies of KIC 6225718 to the frequencies of the best-fitting stellar model, which have been corrected for surface effects. The spherical degrees of the modes are labelled. The uncertainties of the measurements are indicated, the majority of which are too small to be seen. **RIGHT PANEL.** A comparison of observed and (interpolated) theoretical frequency ratios.

ous oscillation modes were presented by Bellinger et al. (2017).

The reason for having two kernels rather than one is that the frequencies of oscillation depend on dynamical variables (pressure, density, and gravity) as well as the adiabatic compressibility  $\Gamma_1 = (\partial \ln P / \partial \ln \rho)_{\text{ad}}$ . Whereas each dynamical variable is directly expressible in terms of the others and thus can be used to eliminate them,  $\Gamma_1$  depends on the equation of state and thus on the composition (and hence the helium abundance) of the stellar plasma. Fortunately, the helium kernel has negligible amplitude throughout the majority of the stellar interior, which effectively isolates differences in the frequencies of the mode to differences in the sound speed. Although deriving the helium kernel comes at the cost of assuming an equation of state, the systematic error caused by this assumption is likely to be much smaller than the uncertainty on the inversion result (Basu & Christensen-Dalsgaard 1997).

As 59 oscillation modes have been detected by *Kepler* in KIC 6225718, we have 59 such equations to work with. This forms the set of equations that we use to determine the differences in  $u'$  between the star and the best-fitting stellar model.

In order to combine the measurements of mode frequencies to produce a measurement of the internal structure, we use the inversion technique known as Subtractive Optimally Localized Averages (SOLA, Pijpers & Thompson 1992, 1994). This method works by combining the  $u'$  kernels in such a way that their combina-

tion, known as the averaging kernel ( $\mathcal{K} = \sum_i c_i K_i^{(u', Y)}$ , where  $\mathbf{c}$  are the coefficients of the linear combination and  $i$  refers to the  $i$ th observed mode of oscillation), only has amplitude near one location, called the target radius ( $r_0$ ). A well-localized averaging kernel represents an instrument for inferring differences in  $u'(r_0)$  between the star and the model. We achieve this by optimizing  $\mathbf{c}$  such that the resulting averaging kernel best resembles a function of our choosing, called the target kernel, which we choose to be a Gaussian peaked at  $r_0$  modified such that it goes smoothly to zero at the core (e.g., Basu & Chaplin 2017). Provided the averaging kernel is well-localized at the target radius and integrates to unity, and furthermore if that same combination of  $Y$  kernels (called the cross-term kernel,  $\mathcal{C} = \sum_i c_i K_i^{(Y, u')}$ ) has negligible amplitude everywhere, then an estimate of the structure of the star can be obtained by applying that same linear combination to the relative differences in the mode frequencies. In other words,

$$\sum_i c_i \frac{\delta \nu_i}{\nu_i} = \left\langle \frac{\delta u'}{u'} \right\rangle (r_0) \simeq \int \mathcal{K} \frac{\delta u'}{u'} dx \quad (2)$$

where the angled brackets represent a weighted average, with the averaging kernel being the weighting function. Surface effects are suppressed by enforcing

$$\sum_i c_i F_{\text{surf}}(\nu_i) = 0 \quad (3)$$

where we adopt the Ball & Gizon (2014) two-term correction for the surface term  $F_{\text{surf}}$ . The uncertainty in



the solution is

$$e^2 = \sum_i c_i^2 \sigma_i^2 \quad (4)$$

where  $\sigma_i$  is the observational uncertainty of the frequency of mode  $i$ . Thus when optimizing the coefficients  $\mathbf{c}$  subject to the aforementioned constraints, we tune free parameters which balance the agreement of the averaging kernel with the target kernel against the resulting amplitude of the cross-term kernel as well as the magnification of the uncertainty in the results (e.g., [Rabello-Soares et al. 1999](#)).

The results of the asteroseismic inversion are shown in Figure 3. Well-localized averaging kernels were able to be formed at target radii  $0.06 - 0.3R$ , probing the radiative interior of the star just beyond the convective core boundary ( $0.034R$ ). The cross-term kernels have negligible amplitude everywhere, and the contributions at the surface are small.

Substantial differences between the structure of the star and the structure of the model as well as a large gradient are apparent in the inversion result. As the results of the inversion at different target radii are correlated (see Figure 4) since they are each estimated using the same data, it is not trivial to assess the significance of this slope. In order to account for these correlated uncertainties, we performed 10 000 Monte Carlo realizations of the uncertainty in the frequencies, and obtained  $d/dx(\delta u'/u') = -1.78 \pm 0.84$  as indicated in the figure, where  $x = r/R$ . Thus the slope differs significantly from zero at a level of more than  $2\sigma$ . This indicates that there are significant differences between the structure of the star and the structure of the best-fitting stellar model.

#### 4. ALTERNATIVE MODELS

Having found that there are differences between the star and the stellar model, we now seek to understand the source of these differences. This can be achieved through a comparison of the reference model and models which have been constructed differently. We consider four such possibilities: the effect of the radius-to-mass ratio of the reference model, the effect of the input physics (diffusion and overshoot), the effect of the evolution code and fitting technique, and the effect of the surface term correction.

##### 4.1. Effect of mass and radius

The best-fitting model of KIC 6225718 was selected from the mode of the joint posterior distribution. Yet this is not the only model consistent with the observations; other models with a higher or lower mass or radius are not ruled out. Figure 5 shows a comparison of the  $u'$  structure between the reference model and two mod-

els which differ by  $\pm 1\sigma$  ( $0.03 R_\odot/M_\odot$ ) in the radius-to-mass ratio. The resultant differences are small, and thus we can conclude from this comparison that differences in the global parameters of the model are unlikely to be the cause of the discrepancies seen in the inversion result. We furthermore performed the inversion with these models as reference and obtained the same result (not pictured).

##### 4.2. Effect of input physics

In order to assess whether a different set of input physics would resolve the discrepancies, we computed three more grids of models which include the effects of (I) convective core overshoot, (II) element diffusion, and (III) both of these.

We used the classical step formulation of convective core overshooting with an overshooting parameter  $\alpha_{\text{ov}} = 0.2$ . As is default in MESA, overshoot is treated with a radiative temperature gradient. We do not consider the effects of convective envelope undershooting.

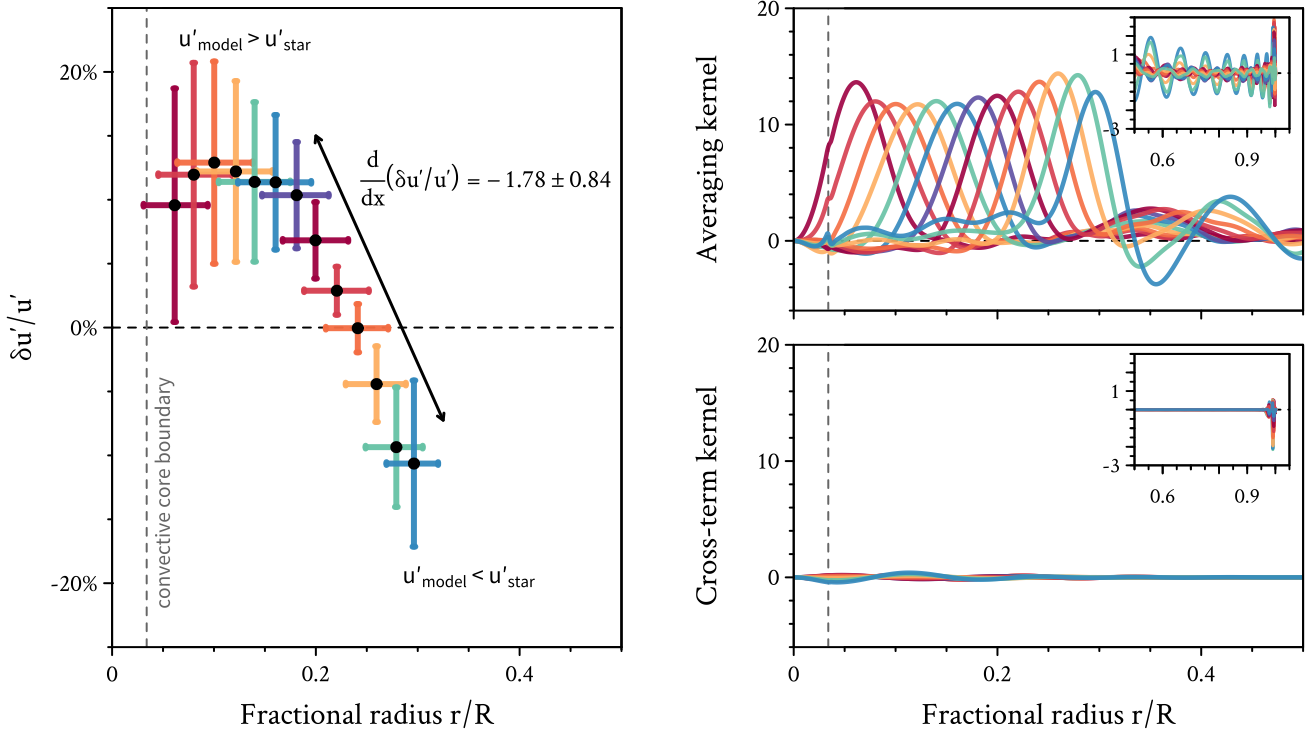
Since gravitational settling in higher-mass models leads to the unobserved consequence of zero-metallicity atmospheres unless it is resisted by mass loss or radiative levitation (e.g., [Deal et al. 2018](#)), the computation of which is computationally expensive, we tapered off diffusion for evolutionary tracks with  $M > 1.25 M_\odot$  according to the equation given by [Viani & Basu \(2017\)](#). Despite the unphysical nature of this prescription, the star under investigation here is of a low enough mass that the diffusion-tapered models are irrelevant. The neglect of radiative levitation should not make a difference to the result as its main effects are in the outer layers of the star. The remaining aspects of the models were unchanged. We then used SPI to find the best-fitting model for each of these grids.

Figure 5 compares the  $u'$  profiles of these models with the reference model. It can be seen that the differences caused by a change of input physics do not produce a signal of the same magnitude seen in the inversion result. We again inverted using these models as reference and again obtained essentially the same result. Furthermore, the mode frequencies of these models have even larger deviations with respect to the observations than the reference model. Thus this is an unlikely culprit.

##### 4.3. Effect of evolution code & fitting technique

Figure 5 compares the structure of the MESA/SPI model with the best-fitting model obtained using the Aarhus Stellar Evolution Code (ASTEC, [Christensen-Dalsgaard 2008a](#); [Silva Aguirre et al. 2017](#)). The likelihood-weighted properties from ASTEC give a mass, radius, and age that are all within  $1\sigma$  of the MESA/SPI





**Figure 3.** Result of the asteroseismic structure inversion. LEFT PANEL. Relative difference between the dimensionless squared isothermal sound speed in the star and the best-fitting stellar model, in the sense of  $(\text{model} - \text{star})/\text{model}$ . A strong gradient can be seen, the slope of which is indicated. The horizontal uncertainties correspond to the width of the averaging kernel. The colors are for ease of identifying the corresponding averaging kernel. TOP RIGHT PANEL. Averaging kernels colored by target radius, corresponding to the inversion results in the left panel. The convective core boundary at  $x = r/R \simeq 0.035$  is visible as a small bump in the averaging kernels and is indicated with a dashed gray line. The inset figure shows the outer layers of the star. Note the differences in scale. BOTTOM RIGHT PANEL. Cross-term kernels for the inversion. For ease of comparison, the scales are set to match those of the averaging kernels. The inset again shows the behavior in the outer layers. The convective core boundary is indicated.

estimates. The radius-to-mass ratio of the best-fitting ASTEC model is approximately the same as that of the best-fitting MESA model. We again find that an inversion using the ASTEC model as reference produces the same result as with the MESA model.

#### 4.4. Effect of surface term correction

As a final test, we consider a model with a surface structure artificially modified in a way such that it does not show a systematic error between the observed and theoretical model frequencies (i.e., no surface effect). We achieve this by changing the adiabatic compressibility in the near surface layers. Figure 6 shows  $\Gamma_1$  in the modified model and a comparison of its oscillation mode frequencies, confirming that the (non-physical) modification to the near-surface  $\Gamma_1$  profile has eliminated surface effects. An inversion with this modified model, however, again yields the same result. As the amplitude of the av-

eraging and cross-term kernels are small near the surface anyway (Figure 3), this result was expected.

## 5. CONCLUSIONS

We have presented an asteroseismic investigation of the *Kepler* target KIC 6225718. After obtaining a best-fitting stellar model of this star, we found that the asteroseismic properties of the star differ from those of the model, even after applying surface term corrections to the theoretical mode frequencies. This implies that the internal structure which is predicted by stellar evolution theory is not correct. We then performed an inverse analysis of the oscillation frequencies to determine the dimensionless internal structure of the star. Comparing this structure of the star with the structure of the model, we found there are significant differences in the structure of the radiative interior near to the convective core boundary. We investigated whether these differences could stem from having an incorrect mass



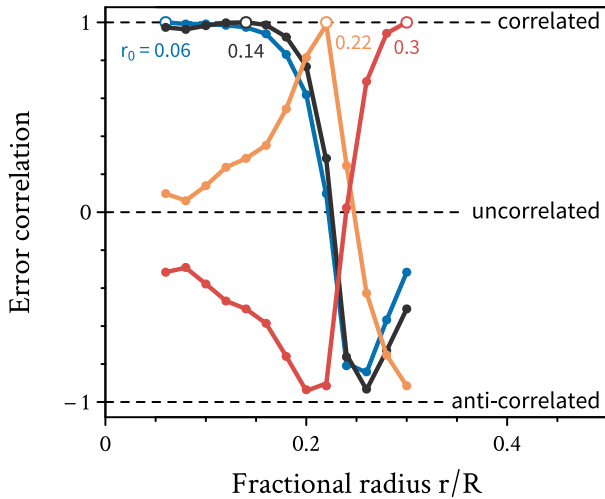


**Figure 4.** Error correlations in the inversion results for four target radii (see Equation 10.38 in Basu & Chaplin 2017). Each curve shows a comparison of the error correlation between the result at that target radius (indicated with an open circle) and all other target radii (closed circles).

or radius in the model, incorrect input physics, incorrect treatment of the surface term, or from the choice of stellar evolution code. In each case however we found that the differences imposed by such an effect are much smaller than the differences that we found between the star and the model. Thus the cause of these discrepancies remains a mystery.

As the speed of sound is inversely related to the mean molecular weight, these results may imply that important internal mixing processes are missing from stellar evolution calculations. While previous studies have indicated the need for additional mixing at the convective core boundary (e.g., Deheuvels et al. 2016), we have found that convective core overshooting is insufficient to explain the internal structure of KIC 622517, and that additional processes are likely to be at work.

We thank the anonymous referee for useful comments. Funding for the Stellar Astrophysics Centre is provided by The Danish National Research Foundation (Grant agreement no.: DNR106). S.H. acknowledges funding from the European Research Council under the European Community’s Seventh Framework Programme (FP7/2007-2013) / ERC grant agreement no 338251 (StellarAges). S.B. acknowledges partial support from NSF grant AST-1514676 and NASA grant NNX13AE70G.

*Software:* ASTEC (Christensen-Dalsgaard 2008a), ADIPLS (Christensen-Dalsgaard 2008b), MESA (Paxton

et al. 2011, 2013, 2015, 2018, 2019), GYRE (Townsend & Teitler 2013; Townsend et al. 2018), R (R Core Team 2014), magicaxis (Robotham 2016), scikit-learn (Pedregosa et al. 2011)



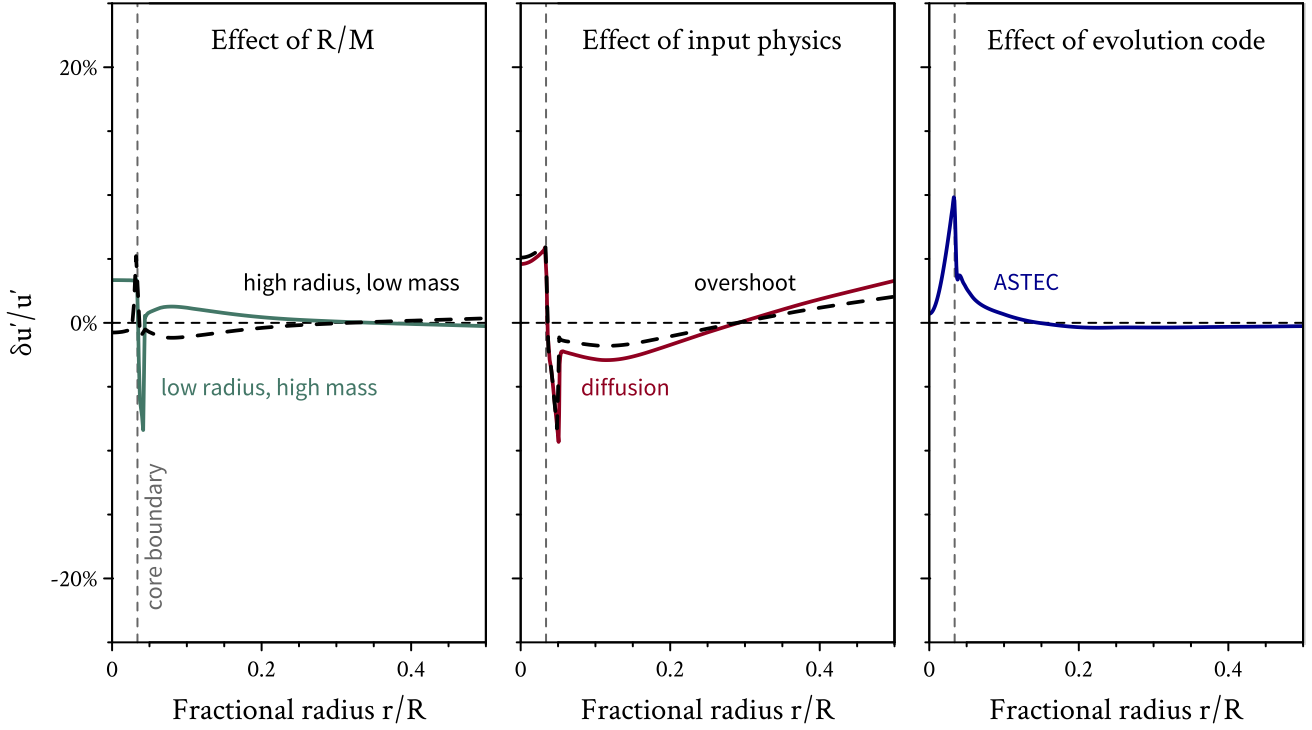


**Figure 5.** Relative difference in dimensionless sound speed between the original model and different models of KIC 6225718. For the purposes of comparison, the axis ranges have been made the same as those in Figure 3. In each case, the differences are smaller than the differences seen between the star and the model. The boundary of the convective core in the original model is indicated. LEFT PANEL. Differences between the original model and models which are higher and lower in their radius-to-mass ratio. MIDDLE PANEL. Differences between the original model and models of differing input physics. A model with both diffusion and overshoot (not pictured) behaves approximately like an average of the two individually. RIGHT PANEL. Differences between the original MESA model and a model made using ASTEC.

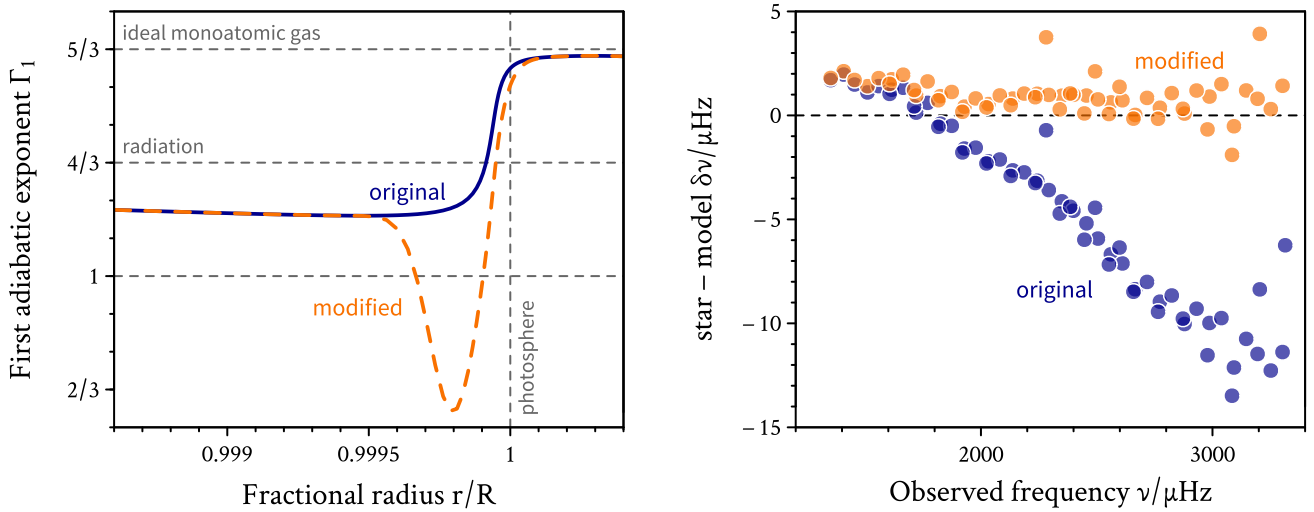


**Figure 6.** LEFT PANEL. A comparison of the near-surface thermal structure of the original model and the model which has been modified to remove surface effects. RIGHT PANEL. A comparison of the mode frequencies of between the star and the two models shown on the left.



## REFERENCES

- Aerts, C., Christensen-Dalsgaard, J., & Kurtz, D. W. 2010, *Asteroseismology* (Springer Science)
- Angelou, G. C., Bellinger, E. P., Hekker, S., & Basu, S. 2017, *ApJ*, 839, 116, doi: [10.3847/1538-4357/aa6a54](https://doi.org/10.3847/1538-4357/aa6a54)
- Ball, W. H., & Gizon, L. 2014, *A&A*, 568, A123, doi: [10.1051/0004-6361/201424325](https://doi.org/10.1051/0004-6361/201424325)
- Basu, S. 2003, *Astrophysics and Space Science*, 284, 153, doi: [10.1023/A:1023223115165](https://doi.org/10.1023/A:1023223115165)
- Basu, S. 2016, *Living Reviews in Solar Physics*, 13, 2, doi: [10.1007/s41116-016-0003-4](https://doi.org/10.1007/s41116-016-0003-4)
- Basu, S., & Chaplin, W. 2017, *Asteroseismic Data Analysis: Foundations and Techniques*, Princeton Series in Modern Obs (Princeton University Press).  
<https://books.google.com/books?id=dQmTAQAACAAJ>
- Basu, S., & Christensen-Dalsgaard, J. 1997, *A&A*, 322, L5
- Bellinger, E. P. 2019, *MNRAS*, 486, 4612, doi: [10.1093/mnras/stz714](https://doi.org/10.1093/mnras/stz714)
- Bellinger, E. P., Angelou, G. C., Hekker, S., et al. 2016, *ApJ*, 830, 31, doi: [10.3847/0004-637X/830/1/31](https://doi.org/10.3847/0004-637X/830/1/31)
- Bellinger, E. P., Basu, S., Hekker, S., & Ball, W. H. 2017, *ApJ*, 851, 80, doi: [10.3847/1538-4357/aa9848](https://doi.org/10.3847/1538-4357/aa9848)
- Bellinger, E. P., Hekker, S., Angelou, G. C., Stokholm, A., & Basu, S. 2019, *A&A*, 622, A130, doi: [10.1051/0004-6361/201834461](https://doi.org/10.1051/0004-6361/201834461)
- Borucki, W. J., Koch, D., Basri, G., et al. 2010, *Science*, 327, 977, doi: [10.1126/science.1185402](https://doi.org/10.1126/science.1185402)
- Christensen-Dalsgaard, J. 2008a, *Ap&SS*, 316, 13, doi: [10.1007/s10509-007-9675-5](https://doi.org/10.1007/s10509-007-9675-5)
- . 2008b, *Ap&SS*, 316, 113, doi: [10.1007/s10509-007-9689-z](https://doi.org/10.1007/s10509-007-9689-z)
- Christensen-Dalsgaard, J., Proffitt, C. R., & Thompson, M. J. 1993, *ApJL*, 403, L75, doi: [10.1086/186725](https://doi.org/10.1086/186725)
- Deal, M., Alecian, G., Lebreton, Y., et al. 2018, *A&A*, 618, A10, doi: [10.1051/0004-6361/201833361](https://doi.org/10.1051/0004-6361/201833361)
- Deheuvels, S., Brandão, I., Silva Aguirre, V., et al. 2016, *A&A*, 589, A93, doi: [10.1051/0004-6361/201527967](https://doi.org/10.1051/0004-6361/201527967)
- Eggleton, P. P., Faulkner, J., & Flannery, B. P. 1973, *A&A*, 23, 325
- Fukunaga, K., & Hostetler, L. 1975, *IEEE Trans. Inf. Theory*, 21, 32
- Gough, D. 1985, *Solar Physics*, 100, 65, doi: [10.1007/BF00158422](https://doi.org/10.1007/BF00158422)
- Gough, D. O., & Thompson, M. J. 1991, *The inversion problem* (University of Arizona Press), 519–561
- Kosovichev, A. G. 1999, *Journal of Computational and Applied Mathematics*, 109, 1
- Lund, M. N., Silva Aguirre, V., Davies, G. R., et al. 2017, *ApJ*, 835, 172, doi: [10.3847/1538-4357/835/2/172](https://doi.org/10.3847/1538-4357/835/2/172)
- Molenda-Żakowicz, J., Sousa, S. G., Frasca, A., et al. 2013, *MNRAS*, 434, 1422, doi: [10.1093/mnras/stt1095](https://doi.org/10.1093/mnras/stt1095)
- Paxton, B., Bildsten, L., Dotter, A., et al. 2011, *ApJS*, 192, 3, doi: [10.1088/0067-0049/192/1/3](https://doi.org/10.1088/0067-0049/192/1/3)
- Paxton, B., Cantiello, M., Arras, P., et al. 2013, *ApJS*, 208, 4, doi: [10.1088/0067-0049/208/1/4](https://doi.org/10.1088/0067-0049/208/1/4)
- Paxton, B., Marchant, P., Schwab, J., et al. 2015, *ApJS*, 220, 15, doi: [10.1088/0067-0049/220/1/15](https://doi.org/10.1088/0067-0049/220/1/15)
- Paxton, B., Schwab, J., Bauer, E. B., et al. 2018, *ApJS*, 234, 34, doi: [10.3847/1538-4365/aaa5a8](https://doi.org/10.3847/1538-4365/aaa5a8)
- Paxton, B., Smolec, R., Schwab, J., et al. 2019, arXiv e-prints. <https://arxiv.org/abs/1903.01426>
- Pedregosa, F., Varoquaux, G., Gramfort, A., et al. 2011, *Journal of Machine Learning Research*, 12, 2825
- Pijpers, F. P., & Thompson, M. J. 1992, *A&A*, 262, L33
- . 1994, *A&A*, 281, 231
- R Core Team. 2014, *R: A Language and Environment for Statistical Computing*, R Foundation for Statistical Computing. <http://www.R-project.org/>
- Rabello-Soares, M. C., Basu, S., & Christensen-Dalsgaard, J. 1999, *Monthly Notices of the Royal Astronomical Society*, 309, 35, doi: [10.1046/j.1365-8711.1999.02785.x](https://doi.org/10.1046/j.1365-8711.1999.02785.x)
- Robotham, A. 2016, *magicaxis: Pretty Scientific Plotting with Minor-Tick and log Minor-Tick Support*.  
<http://CRAN.R-project.org/package=magicaxis>
- Roxburgh, I. W. 2005, *A&A*, 434, 665, doi: [10.1051/0004-6361:20041957](https://doi.org/10.1051/0004-6361:20041957)
- . 2018, arXiv e-prints. <https://arxiv.org/abs/1808.07556>
- Roxburgh, I. W., & Vorontsov, S. V. 2003, *A&A*, 411, 215, doi: [10.1051/0004-6361:20031318](https://doi.org/10.1051/0004-6361:20031318)
- . 2013, *A&A*, 560, A2, doi: [10.1051/0004-6361/201321333](https://doi.org/10.1051/0004-6361/201321333)
- Silva Aguirre, V., Lund, M. N., Antia, H. M., et al. 2017, *ApJ*, 835, 173, doi: [10.3847/1538-4357/835/2/173](https://doi.org/10.3847/1538-4357/835/2/173)
- Townsend, R. H. D., Goldstein, J., & Zweibel, E. G. 2018, *MNRAS*, 475, 879, doi: [10.1093/mnras/stx3142](https://doi.org/10.1093/mnras/stx3142)
- Townsend, R. H. D., & Teitler, S. A. 2013, *MNRAS*, 435, 3406, doi: [10.1093/mnras/stt1533](https://doi.org/10.1093/mnras/stt1533)
- Viani, L., & Basu, S. 2017, in *European Physical Journal Web of Conferences*, Vol. 160, *Seismology of the Sun and the Distant Stars*, 05005, doi: [10.1051/epjconf/201716005005](https://doi.org/10.1051/epjconf/201716005005)